sustainability

MDPI

Article

Remaining Useful Life Prediction for Lithium-Ion Batteries Based on the Partial Voltage and Temperature

Yanru Yang [1,2], Jie Wen [1,*], Jianyu Liang [3], Yuanhao Shi [1], Yukai Tian [1] and Jiang Wang [1]

[1] School of Electrical and Control Engineering, North University of China, Taiyuan 030051, China
[2] Shanghai Research Institute for Intelligent Autonomous Systems, Tongji University, Shanghai 200092, China
[3] School of Data Science and Technology, North University of China, Taiyuan 030051, China
* Correspondence: wenjie@nuc.edu.cn

Abstract: Remaining useful life (RUL) prediction is vital to provide accurate decision support for a safe power system. In order to solve capacity measurement difficulties and provide a precise and credible RUL prediction for lithium-ion batteries, two health indicators (HIs), the discharging voltage difference of an equal time interval (DVDETI) and the discharging temperature difference of an equal time interval (DTDETI), are extracted from the partial discharging voltage and temperature. Box-Cox transformation, which is data processing, is used to improve the relation grade of HIs. In addition, the Pearson correlation is employed to evaluate the relationship degree between HIs and capacity. On this basis, a local Gaussian function and a global sigmoid function are utilized to improve the multi-kernel relevance vector machine (MKRVM), whose weights are optimized by applying a whale optimization algorithm (WOA). The availability of the extracted HIs as well as the accuracy of the RUL prediction are verified with the battery data from NASA.

Keywords: lithium-ion battery; remaining useful life; state of health; voltage; temperature

Citation: Yang, Y.; Wen, J.; Liang, J.; Shi, Y.; Tian, Y.; Wang, J. Remaining Useful Life Prediction for Lithium-Ion Batteries Based on the Partial Voltage and Temperature. *Sustainability* **2023**, *15*, 1602. https://doi.org/10.3390/su15021602

Academic Editors: Jiangong Zhu, Weibo Hua and Guiying Tian

Received: 13 December 2022
Revised: 5 January 2023
Accepted: 10 January 2023
Published: 13 January 2023

1. Introduction

Due to the high energy density, low self-discharge rate, and long service life of lithium-ion batteries, they are the energy supply source for many important pieces of equipment or systems and have undergone vigorous development in the relevant power battery and energy storage markets [1]. However, battery failure may result in system performance degradation, or even catastrophic equipment failure and damage. Degradation modeling, remaining useful life (RUL) prediction, and health management for batteries will greatly improve the capability of the energy storage and power system. Therefore, RUL prediction has very important practical value and significance for lithium-ion batteries. The health condition of batteries mainly includes state of health (SOH), state of charge (SOC), RUL, etc. [2,3]. The role of RUL is very important in the safe and reliable working of the system [4–6]. As the cycle increases, the loss of active lithium ions and electrode active materials leads to capacity degradation, until the battery fails. If the health information of a battery can be established in advance, it can be replaced before it reaches the failure threshold, to avoid safety accidents [7].

To establish the health condition of the lithium-ion battery, the model-based method is proposed first. For example, Prada et al. proposed an electrochemical model to simulate capacity degradation [8]. Thomas et al. explored the physical model considering degradation rate, which improves the ability of the model to adapt to non-isothermal degradation conditions and predicts the cell life [9]. In addition, Li et al. proposed the extended single-particle model to estimate the SOC as well as lithium-ion concentrations and potentials, and the estimation accuracies of the model were then verified using numerical validation tests [10]. Li et al. proposed a degradation-conscious high-fidelity electrochemical–thermal

model that performs excellently in terms of accuracy, computational speed and robustness [11]. However, the deterioration mechanism of lithium-ion batteries in operation time is complicated and it is difficult to establish an accurate model [12].

To reduce the error in the modeling process, data-driven models have extensively worked in the prognostic strategy of RUL prediction [13–15]. Zhang et al. developed a deep-learning prognostic with the capacity to obtain the RUL prediction for lithium-ion batteries, where the optimization of parameters was based on an online validation, and the performance of long-horizon prediction was tested with a battery dataset [16]. To improve computing efficiency without being time-consuming, Yu et al. employed a decomposition method to divide capacity into trend and recovery, and then used Gaussian process regression (GPR) to obtain the RUL prediction [17]. To overcome the difficulty of measuring capacity [18], Li et al. developed a relevance vector machine (RVM) method, extracting the mean entropy to achieve RUL prediction [19]. In addition, Sun et al. proposed a health indicator (HI), which incorporates capacitance, resistance and other information, and a case study was then carried out to validate the RUL of lithium batteries [20]. Instead of only one HI, Zhao et al. proposed two real-time measurable HIs and developed support vector regression (SVR) to obtain capacity and RUL prediction [21]. Widodo et al. proposed two reasonable prognostics to predict the lithium-ion battery SOH based on the HI extracted from discharge voltage, which indicated RVM performed better relative to SVR [22]. Since RVM does not require the kernel function to be positive definite, Zhang et al. proposed a multi-kernel relevance vector machine (MKRVM) so that the precise prediction of the capacity and the weights of MKRVM are optimized using a particle swarm optimization (PSO) algorithm. [23]. What is more, RVM also provided probabilistic interval prediction, which makes the results more convincing [24,25]. Liu et al. presented a HI extraction, and on the basis of the HI obtained, an optimization method was used, and they built the RVM model to achieve the RUL prediction prognostic [26].

However, the models mentioned in the above literature only involved voltage influence on capacity degradation. Temperature also affects the rate of chemical reactions, thereby affecting the activity and electrolyte performance of the electrode material inside the battery [27,28]. Lu et al. studied the operating temperature effects on the lithium-ion battery in [29], where the experiments showed that the performance of the model can be developed in a suitable temperature range. In addition, Tang et al. developed a general model that illustrated temperature and degradation, and is effective for battery management [30]. Kong et al. proposed a voltage-temperature HI extraction prognostic for health conditions and battery lifetime prediction [31].

However, there are few RUL prediction models which take temperature into consideration, so the temperature is extracted as one of HIs to predict the RUL for lithium-ion batteries in this paper. From the perspective of indirect forecasting, an online RUL prognostic, which considers the indirect information in operation process, is proposed for the capacity and RUL prediction of lithium-ion batteries. We extracted HIs from discharging process. Box-Cox was applied to strengthen the line relationship between HIs and capacity. Taking local regeneration into account, we used local Gaussian and the global sigmoid function as the fusion kernel function of RVM, whose weights were optimized by using the whale optimization algorithm (WOA). Finally, we provided RUL prediction results consisting of a deterministic prediction and interval with confident probability. The main contributions of this paper are as follows: (1) to solve capacity measurement difficulties and use the indirect prediction method, the discharging voltage difference of an equal time interval (DVDETI) and the discharging temperature difference of an equal time interval (DTDETI) were extracted as HIs for RUL prediction; (2) to strengthen the relationship between the extracted HIs and capacity, the raw HIs was transformed with Box-Cox and determined the threshold of HIs; (3) to avoid local optimum, WOA was used to optimize the kernel function weights and parameters of MKRVM.

The structure of this paper is as follows. The methodology in this paper is introduced in Section 2. The experimental data, application of the methodology, and the correlation

between HIs and capacity are shown in Section 3. In Section 4, the analysis of one-step and five-step capacity degradation prediction and the RUL results for lithium-ion batteries are presented. Finally, the conclusion of this paper is given in Section 5.

2. Methodology

2.1. Box-Cox

In order to use HI to make a better expression of battery capacity degradation, which is the extracted raw HIs that keep linearity with capacity, we performed Box-Cox transformation on HI. The Box-Cox transformation on HI is described as follows.

2.1.1. Box-Cox Transformation

A linear regression model can be expressed as [32,33]:

$$\begin{gathered} y_i = \beta_0 + \beta_1 x_{i1} + \beta_2 x_{i2} + \ldots, + \beta_q x_{iq} + \varepsilon_i \\ \varepsilon_i \backsim N\left(0, \sigma^2\right), i = 1, 2, \ldots, n \end{gathered} \tag{1}$$

where, q is the number of variables, $\beta_0, \beta_1, \ldots, \beta_q$ are the coefficients, and n is the size of data, through the transformation of the dependent variable.

The Box-Cox transformation is

$$y(\lambda) = \begin{cases} \frac{y_i^{\lambda} - 1}{\lambda}, & if\ \lambda \neq 0; \\ \ln(y_i), & if\ \lambda = 0; \end{cases} \tag{2}$$

The corresponding inverse transformation is

$$y = \begin{cases} (\lambda y(\lambda) + 1)^{1/\lambda}, \lambda \neq 0 \\ \exp(y(\lambda)), \lambda = 0 \end{cases} \tag{3}$$

where, the transformation parameter λ determines the form of transformation and needs to be calculated. The liner model also can be expressed as

$$y_{(i)}(\lambda) = \beta_0 + \beta_1 x_{i1}^{\lambda} + \beta_2 x_{i2}^{\lambda} +, \ldots, + \beta_q x_{iq}^{\lambda} + \varepsilon_i \tag{4}$$

2.1.2. Parameter Identification for Box-Cox Transformation

The parameter λ needs to be found according to maximum likelihood or Bayesian methods. We use maximum likelihood estimation in this paper.

Assume that $\varepsilon_i \backsim N\left(X\beta, \sigma^2 I\right)$ and according to (4), we have the following joint probability density function of $y(\lambda)$

$$f(y(\lambda)) = \frac{\exp\left(-\frac{1}{2\sigma^2}(y(\lambda) - X\beta)^{\mathrm{T}}(y(\lambda) - X\beta)\right)}{(2\pi\delta^2)^{\frac{n}{2}}} \tag{5}$$

based on which the likelihood function is

$$L\left(\beta, \delta^2, \lambda \middle| y, X\right) = \frac{\exp\left(-\frac{1}{2\delta^2}(y(\lambda) - X\beta)^{\mathrm{T}}(y(\lambda) - X\beta)\right)}{(2\pi\delta^2)^{\frac{n}{2}}} J(\lambda, y) \tag{6}$$

where $J(\lambda, y) = \prod_{i=1}^{n} \left| \frac{dy_i^{(\lambda)}}{dy_i} \right| = \prod_{i=1}^{n} y_i^{\lambda - 1}$ is the Jacobian of the transformation from y to $y(\lambda)$.

Taking the partial derivatives of β and σ^2, respectively, and setting the derivative function to zero, we have

$$\hat{\beta}(\lambda) = \left(X^{\mathrm{T}}X\right)^{-1} X^{\mathrm{T}} y(\lambda) \tag{7}$$

$$\hat{\delta}^2(\lambda) = \frac{\left(y(\lambda) - X\beta^{\mathrm{T}}\right)(y(\lambda) - X\beta)}{n} \tag{8}$$

Place (7) and (8) into (6), we have the maximum of likelihood function

$$L_{\max}(\lambda) = (2\pi)^{-2/n}\left[\delta^2(\lambda)\right]^{-n/2} J(\lambda, y) \tag{9}$$

In order to simplify the calculation of the parameter λ, take the logarithm of both sides of (9), then we have

$$\log(L_{\max}(\lambda)) = -\frac{2}{n}\log(2\pi) - \frac{n}{2}\log\left(\hat{\delta}^2(\lambda)\right) + (\lambda - 1)\sum_{i=1}^{n}\log(y_i) \tag{10}$$

Maximizing $\log(L_{\max}(\lambda))$ is equal to maximizing $g(\lambda)$:

$$g(\lambda) = -\frac{n}{2}\log(\hat{\sigma}(\lambda)) + (\lambda - 1)\sum_{i=1}^{n}\log(y_i) \tag{11}$$

Through the transformation of the dependent variable, the transformed vector $y(\lambda)$, whose explanation of the model interpretation is better, the error obeys the normal distribution, and each error is equal in variance and independent of each other.

2.2. MKRVM

Given an input vector $\mathbf{x}$, the conditional probability distribution of the target variable t can be written as [34]:

$$p(t|\mathbf{x}, \mathbf{w}, \beta) = \mathcal{N}\left(t\middle|y\left((\mathbf{x}), \beta^{-1}\right)\right) \tag{12}$$

where $\beta = \sigma^{-2}$ is noise precision, and the mean value is given by a linear model which can be expressed as

$$y(\mathbf{x}) = \sum_{i}^{N} w_n \phi_i(\mathbf{x}) = \mathbf{w}^{\mathrm{T}}\phi(\mathbf{x}) \tag{13}$$

with fixed nonlinear basis functions $\phi_i(\mathbf{x})$. Given a set of N observations of the input vector $\mathbf{x}$, denoted as the data matrix $\mathbf{X}$, the corresponding target values are $\mathbf{t} = (t_1, \ldots, t_N)^{\mathrm{T}}$. Therefore, the likelihood function is

$$p(\mathbf{t}|\mathbf{X}, \mathbf{w}, \beta) = \prod_{n}^{N} p\left(t_n\middle|\mathbf{x}_n, \mathbf{w}, \beta^{-1}\right) \tag{14}$$

A prior distribution over the parameter vector $\mathbf{w}$ is then introduced to avoid overfitting, which is considered a zero-mean Gaussian prior As well as a separate hyperparameter α_i response to weight w_i. The weight prior can therefore be expressed as

$$p(\mathbf{w}|\boldsymbol{\alpha}) = \prod_{i=1}^{M}\mathcal{N}\left(w_i\middle|0, \alpha_i^{-1}\right) \tag{15}$$

where α_i represents $(\alpha_1, \ldots, \alpha_M)^{\mathrm{T}}$, $M = N + 1$. So, the solution to w is transformed into the solution to α, when α tends to infinity, the posterior distribution of the corresponding weight parameter is zero.

When calculating the posterior distribution, it is proportional to the product of the likelihood function and the prior distribution. The posterior probability distribution is a Gaussian distribution because of its conjugate nature, and the posterior probability distribution form can be obtained:

$$p(\mathbf{w}|\mathbf{t}, \mathbf{X}, \boldsymbol{\alpha}, \beta) = \mathcal{N}(\mathbf{w}|\mathbf{m}, \Sigma) \tag{16}$$

where the mean and variance are

$$\mathbf{m} = \beta \Sigma \Phi^{\mathrm{T}} \mathbf{t} \tag{17}$$

$$\Sigma = \left(\mathbf{A} + \beta \Phi^{\mathrm{T}} \Phi \right)^{-1} \tag{18}$$

where Φ is an $N \times M$ design matrix with $\Phi = [\phi(x_1), \phi(x_2), \ldots \phi(x_n)]^{\mathrm{T}}$ and $\Phi(x_n) = [1, K(x_n, x_1), K(x_n, x_2), \ldots K(x_n, x_n)]^{\mathrm{T}}$, we have $\mathbf{A} = \mathrm{diag}(\alpha_i)$.

The values of $\boldsymbol{\alpha}$ and β are calculated with type-2 maximum likelihood, in which we maximize the marginal likelihood function:

$$p(\mathbf{t}|\mathbf{X}, \boldsymbol{\alpha}, \beta) = \int p(\mathbf{t}|\mathbf{X}, \mathbf{w}, \beta) p(\mathbf{w}|\boldsymbol{\alpha}) \mathrm{d}\mathbf{w} \tag{19}$$

Simply setting the derivatives of the marginal likelihood to zero and obtaining the following results, repeat the above calculation process until the maximum number of iterations is reached. In this paper, the maximum number of iterations is set to 1000.

$$\alpha_i^{new} = \frac{\gamma_i}{m_i^2} \tag{20}$$

$$(\beta^{new})^{-1} = \frac{\|\mathbf{t} - \Phi \mathbf{m}\|^2}{N - \Sigma_i \gamma_i} \tag{21}$$

$$\gamma_i = 1 - \alpha_i \Sigma_{ii} \tag{22}$$

With a new input $\mathbf{x}$, the output distribution on t is

$$p(t|\mathbf{x}, \mathbf{X}, \mathbf{t}, \boldsymbol{\alpha}^*, \beta^*) = \int p(t|\mathbf{x}, \mathbf{w}, \beta^*) p(\mathbf{w}|\mathbf{X}, \mathbf{t}, \boldsymbol{\alpha}^*, \beta^*) \mathrm{d}\mathbf{w} = \mathcal{N}\left(t \middle| \mathbf{m}^{\mathrm{T}} \phi(\mathbf{x}), \sigma^2(\mathbf{x}) \right) \tag{23}$$

The multi-kernel model has higher flexibility than a single kernel function [35]. In the context of multi-kernel mapping, the high-dimensional space becomes a combined space composed of multiple feature spaces. Since the combined space fully uses the different feature mapping capabilities of each basic kernel, different feature components of heterogeneous data can be resolved through corresponding kernel functions. In addition, the kernel function is mainly divided into global and local kernel function [36,37]. Gaussian and sigmoid kernel function, as representatives of the global kernel function and local kernel function, respectively, have been widely used in machine-learning methods and neural networks. The Gaussian kernel function works excellently in extracting the local property of the sample, which is also called the local Gaussian kernel function. In addition, compared to the polynomial kernel function, the excellent global properties based on the sigmoid kernel function have been proved in the performance of classification. Considering the characteristics of Gaussian and sigmoid kernel function, using the fusion kernel function can reduce the kernel parameters and the complexity of the RVM model as much as possible, and give the kernel function both global and local characteristics. Combining multiple kernel functions with different characteristics will result in a function which contains the overall advantage of each kernel function. The way the multi-kernel function is formed makes the multi-kernel function more accurate and stronger in its mapping or classification capabilities, especially for learning problems such as classification and regression with more complex distribution structures of sample data in practical applications. The advantages of multi-kernel function learning are obvious. Therefore, we chose the fusion of Gaussian and sigmoid kernel function to improve the MKRVM performance, and the fusion kernel function is

$$K = \sum_{j=1}^{n} m_j K_j, m_j \geq 0, \sum_{j=1}^{n} m_j = 1 \tag{24}$$

where K_j and m_j denote the kernel function and weight coefficient, respectively.

The Gaussian kernel function is [38]:

$$K_1(x, x_n) = \exp\left(-\frac{\|x - x_n\|^2}{2d^2}\right) \tag{25}$$

where d is the bandwidth, which controls the radial range of action.

The sigmoid kernel function can be expressed as follows [39]

$$K_2(x, x_n) = \tan h\left(tx^{\mathrm{T}}x_n + c\right) \tag{26}$$

where t is a scalar and is c displacement. In addition, WOA has shown good performance in other model optimizations [40,41]. In this paper, WOA is used to improve the convergence speed of MKRVM, as well as the accuracy of the algorithm.

2.3. WOA

WOA, inspired by the hunting behavior of humpback whales, is a new optimization algorithm [42]. The main characteristic of WOA is using the shrink-wrap mechanism and the spiral-up mechanism to realize the local search of the algorithm, and the random learning strategy to realize the global search of the algorithm. It has the advantages of simple processes and fast convergence speed, excellent performance in solving optimization problems, and a wide range of applications. WOA mainly consists of three important stages: encircling prey, bubble-net attacking strategy, and hunting prey.

2.3.1. Encircling Prey

When the humpback whale surrounds the prey, it will choose to swim in the direction of the humpback whale with the best position. The humpback whale can identify the position of the prey and surround it, and its position update can be expressed as

$$D = |C \cdot X^*(t) - X(t)| \tag{27}$$

$$X(t+1) = X^*(t) - A \cdot D \tag{28}$$

where t denotes current iteration, X^* is the best whale position vector so far, X is vector of current whale, A and C are coefficient vectors and can be updated as follows:

$$A = 2a \cdot r - a \tag{29}$$

$$C = 2 \cdot r \tag{30}$$

where r is random vector in $[0, 1]$, and a changes from 2 to 0 in the search process, namely:

$$a = 2 - \left(\frac{2t}{t_{\max}}\right) \tag{31}$$

2.3.2. Bubble-Net Attacking Strategy

Shrinking encircling and spiraling updating is contained in the bubble-net attacking strategy.

Shrinking encircling: The behavior achieved by reducing a in (30). The process is achieved by reducing the value of a in the iterative process. That is, the set random number A defined in $[-1, 1]$, another definition of the new location of the search agent is any location between the current agent and the best agent.

Spiraling updating: This method first calculates the distance between the whale and the prey located at (X, Y) and (X^*, Y^*), respectively, and then establishes a spiral between the positions of the whale and the prey equation to simulate the spiral motion of humpback whales. The behavior is shown as follows:

$$D' = |X^*(t) - X(t)| \tag{32}$$

$$X(t+1) = D' \cdot e^{bl} \cdot \cos(2\pi l) + X^*(t) \tag{33}$$

where D′ indicates the distance from the *i*th search agent to target, l is a random vector and $l \in [-1, 1]$, and b is a constant.

Assuming that the probability of shrinking encircling or spiraling updating is 50% to update the location of the whale in the optimization process, this behavior can be expressed as

$$X(t+1) = \begin{cases} X^*(t) - A \cdot D & if\ p < 0.5 \\ D' \cdot e^{bl} \cdot \cos(2\pi l) + X^*(t) & if\ p > 0.5 \end{cases} \tag{34}$$

2.3.3. Search for Prey

In addition, the whale will randomly choose whether to swim toward the best position of the whale or randomly choose a whale as its target and approach it. Based on each other's location, the behavior can be written as

$$D = |C \cdot X_{rand}(t) - X(t)| \tag{35}$$

$$X(t+1) = X_{rand}(t) - A \cdot D \tag{36}$$

where $\vec{X}_{rand}$ is a random position. If $|A| \geq 1$, the randomly selected whale position is used to update the position of other whales, to find a more suitable prey to realize the global search. The flowchart of WOA is provided in Figure 1.

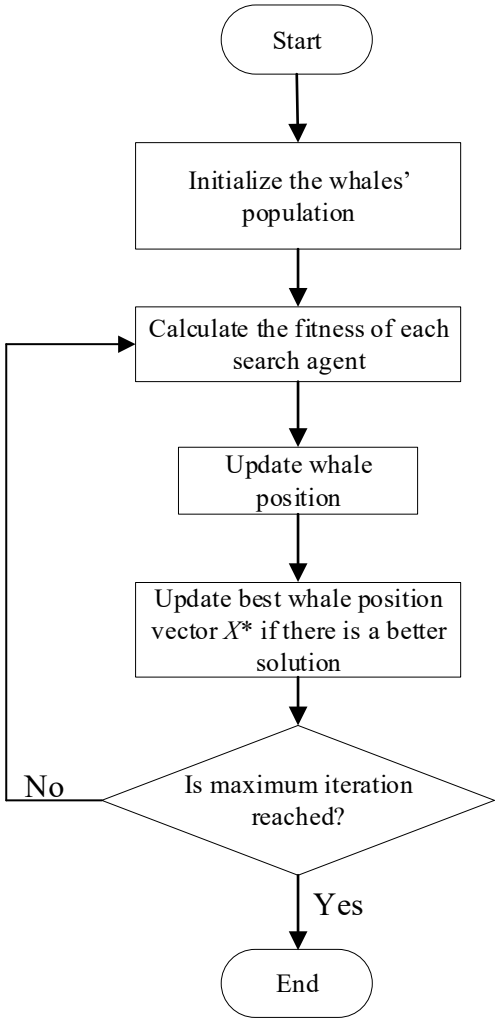

Figure 1. Flowchart of WOA.

2.4. Structure of RUL Framework

The structure of WOA-MKRVM is shown in Figure 2, and the details are presented as follows:

1. Data analysis: Especially in the discharging process. The DVDETI and DTDETI are extracted from the discharging voltage and temperature;
2. Box-Cox Transformation: The DVDETI and DTDETI to get HI1 and HI2 based on the Box-Cox method. Pearson is used to evaluate the correlation degree between capacity and HIs;
3. WOA-MKRVM model training: Historical HIs are chosen as inputs, and the HI responds to the output. The input can be expressed as $X_t^i = \{H_{t-i}\}$, $i = 1, 2, \ldots, n$, n is the length of segment, X_t^i denotes the normalized input data with i segments at cycle t, the corresponding output is $\hat{Y}_t = \{\hat{H}_{t+k}\}$, where k stands for the future steps. The model can be trained for HIs prediction and RUL prediction. Figure 2 is the input and output of MKRVM;
4. HIs prediction: Using the trained model to predict future HIs. The recursive prediction process uses the previously output data of WOA-MKRVM predicted as the next input to the model to make predictions;
5. RUL prediction: in the work, RUL refers to the end-of-life (EOL) cycle minus the current cycle. The RUL can be defined as $RUL = Cycle_{start} - Cycle_{EOL}$. The $Cycle_{start}$ is the predicted start cycle, the $Cycle_{EOL}$ is the cycle of EOL. Based on the recursive prediction process, when reaching the HIs threshold of the lithium-ion battery, the corresponding RUL can be calculated.

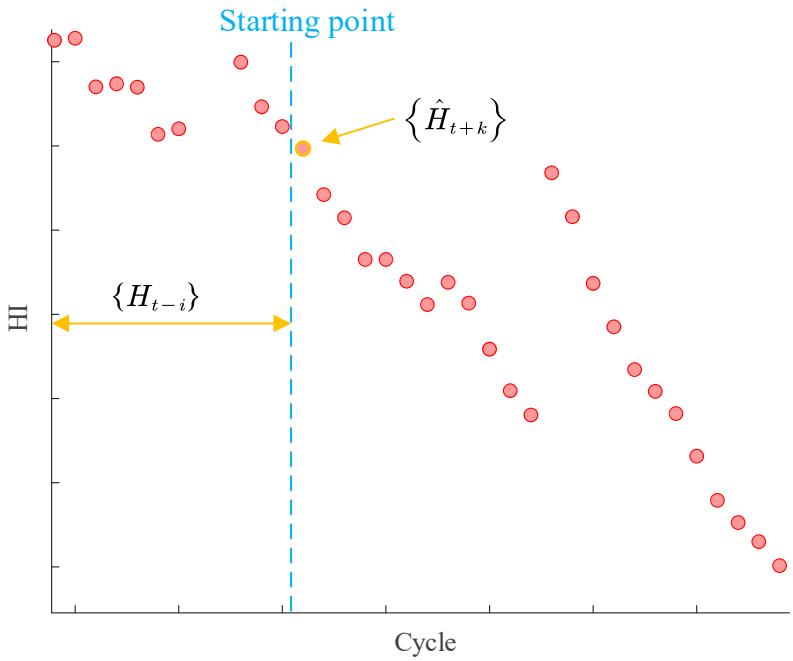

Figure 2. Input and output of MKRVM.

The structure of WOA-MKRVM is shown in Figure 3. The HIs and RUL prediction results were therefore obtained, and the probabilistic prediction results can be provided.

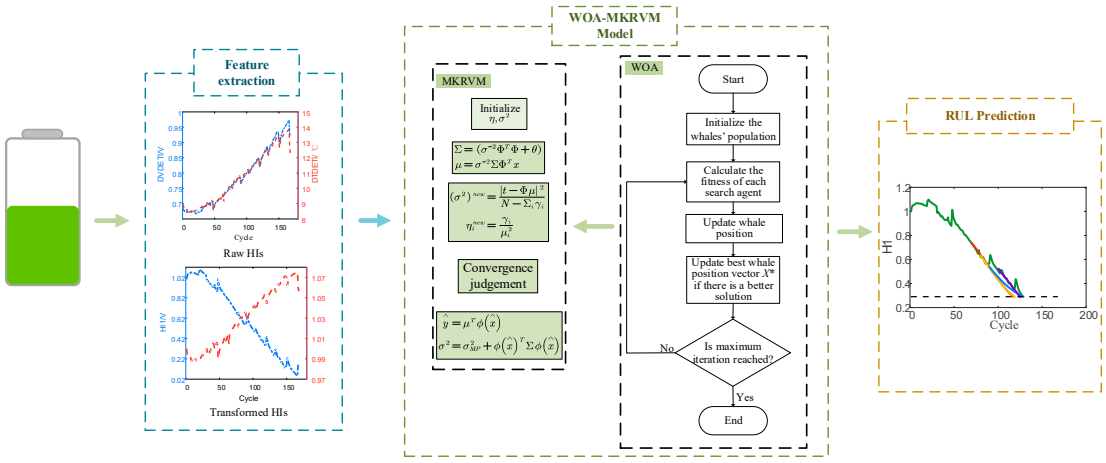

Figure 3. Procedure of WOA-MKRVM.

3. Application of Methodology

3.1. Data Description

The datasets are studied to evaluate the effectiveness of the WOA-MKRVM model, which is from the data repository of the NASA Ames Prognostics Center of Excellence [43]. This data set is tested from a battery prognostic test bed at NASA 18650, whose nominal capacity is 2 Ah and nominal voltage is 3.7 V. In order to compare this study with other research, the popular batteries #5, #6, #7 and #18 were used for this study. The rated capacity of batteries #5, #6, #7, and #18 is 2 Ah. The details are presented in Table 1. The CCC and CCV mean constant current and voltage in the charging process, respectively, while the DCC means constant current in the discharging process, and the EOV denotes the end of the discharging voltage. The set of batteries is always charged with 1.5 A until the voltage of the lithium-ion battery reaches 4.2 V, and they then continue to work at this voltage, ending with current drops to 20 mA, which are tested at room temperature (24 °C). The capacity with the cycle of the four batteries is presented in Figure 4. The cycle of batteries #5, #6, and #7 are 168, and the cycle of battery #18 is 132.

Table 1. Parameters of batteries #5, #6, #7 and #18.

Battery	CCC (A)	CCV (V)	DCC (A)	EOV
#5	1.5	4.2	2	2.7
#6	1.5	4.2	2	2.5
#7	1.5	4.2	2	2.2
#18	1.5	4.2	2	2.5

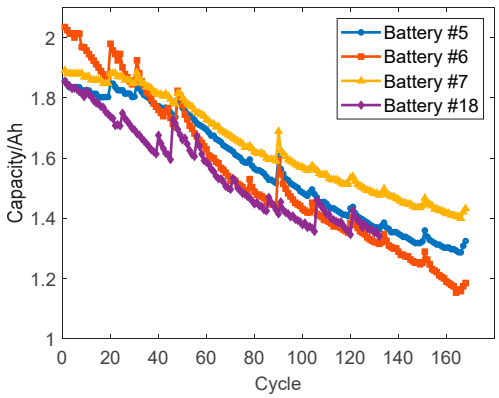

Figure 4. The capacity curves of the four batteries (batteries #5, #6, #7 and #18).

3.2. HI Extraction

There are many factors that affect lithium-ion batteries degradation, such as voltage, current, temperature, depth of discharge, and so on [44–46]. The operating time of a fully charged lithium-ion battery gradually decreases with the charge and discharge cycles, as well as the maximum capacity degradation with cycles. The voltage and temperature curves in the discharge process are shown in Figure 5, from which it is shown that as the cycles increased, at a specific time during discharge, the difference between the initial voltage and the time voltage became larger. The difference between the initial temperature and the real-time temperature also followed the same pattern. Therefore, we can use voltage fall-off and temperature change in a defined time interval to quantify lithium-ion battery degradation.

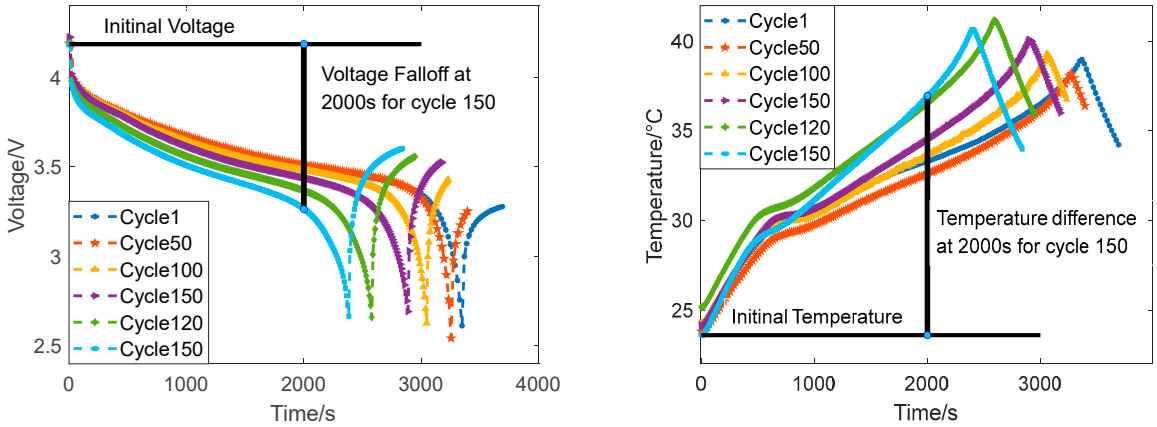

(**a**) (**b**)

Figure 5. Discharge curves: (**a**) Discharge voltage curves; (**b**) Discharge temperature curves.

Taking battery #5 as an example for HIs extraction analysis, the voltage and temperature curve at cycle 100 of battery #5 is shown in Figure 6, from which one can see that the first phase was more able to respond to more information. In the first period, the change of amplitude in the voltage change was greater than in other stages, so it is reasonable to choose the first phases to reflect the capacity degradation of lithium batteries. Moreover, the temperature also followed the same pattern. Therefore, we focused on the battery discharge process to extract the HIs. The time interval start point was 0 s, and endpoint was set as 2000s. The DVDETI and the DTDETI in the *i*th cycle were, respectively:

$$DVDETI_i = V_{t_{\max}} - V_{t_{\min}}, i = 1, 2 \ldots, n \tag{37}$$

$$DTDETI_i = T_{t_{\max}} - T_{t_{\min}}, i = 1, 2 \ldots, n \tag{38}$$

DVDETI series can be expressed as

$$DVDETI = \{DVDETI_1, DVDETI_2, \ldots, DVDETI_n\} \tag{39}$$

DTDETI series can be expressed as

$$DTDETI = \{DTDETI_1, DTDETI_2, \ldots, DTDETI_n\} \tag{40}$$

The HIs are shown in Figure 7. It is clear that the DVDETI and DTDETI increase in amplitude as the cycle increases, and the HIs are strongly correlated with capacity. Thus, the changes in voltage and temperature at defined time intervals not only provide the global trend, but also the local regeneration, which can reflect the degradation of lithium-ion batteries.

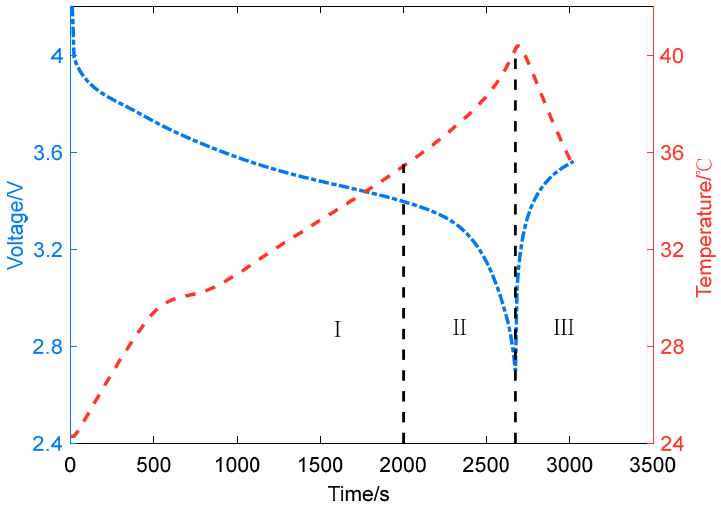

Figure 6. Discharge curve of the 100th cycle (battery #5).

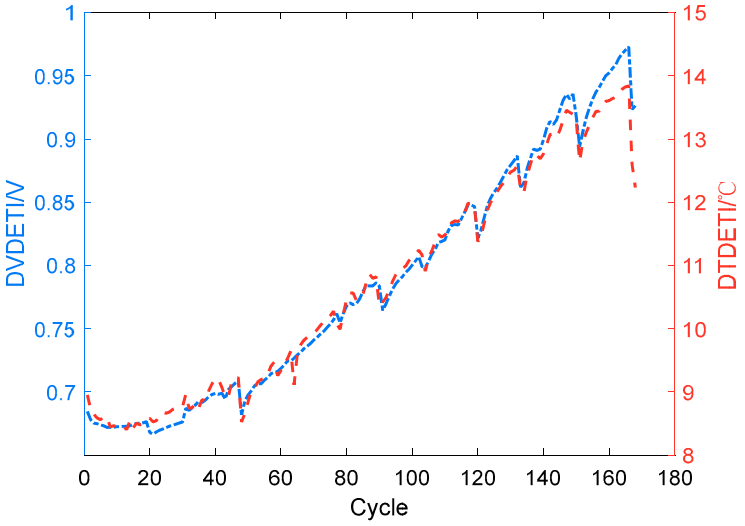

Figure 7. Extracted HIs.

3.3. Box-Cox Transformation

In order to improve the performance of DVDETI and DTDETI, which can better indicate battery capacity degradation, the Box-Cox is used to achieve DVDETI and DTDETI to obtain HI1 and HI2 in this study. In addition, the failure threshold points of HI1 and HI2 after the calculation conversion need to be calculated.

The linear model for the DVDETI, DTDETI and capacity, which is with the identified parameter λ of Box-Cox transformation, are denoted as

$$C = \beta_0 + \beta_1 HI \tag{41}$$

where, HI represents normalization DVDETI or DTDETI.

Based on (41), the failure threshold of HI can be expressed as

$$HI_p = \frac{C_p - \beta_0}{\beta_1} \tag{42}$$

where C_p represents the capacity threshold, and HI_p represents the transformed HI failure threshold.

Therefore, the threshold of Box-Cox transformed HIs can be used as the parameter of the RUL prediction, and it can also be used as the preset condition parameter in actual applications.

Figure 8 is the HIs after Box-Cox. It can be seen that HI1 and capacity show the same trend, while HI2 and capacity have the opposite trend. Next, we will quantify the relationship between HIs and capacity by correlation analysis.

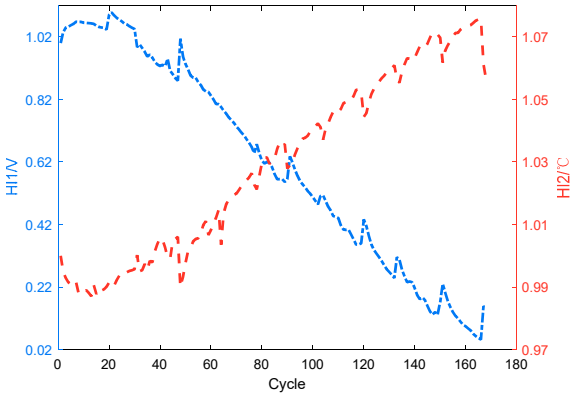

Figure 8. HIs after Box-Cox.

3.4. Correlation Analysis

3.4.1. Qualitative Analysis

To demonstrate the performance of HIs, the correlation between HIs and capacity is analyzed in this paper. Scatter plots of the correlation between DVDETI, DTDETI, and capacity are presented in Figure 9. From this, it can be seen that both DVDETI and DTDETI are positively correlated with capacity, and the linearity between the HI1, HI2, and capacity is improved. Moreover, the HI1 and HI2, which are transformed in this paper, are suitable to be used as features to present the degradation of lithium-ion batteries.

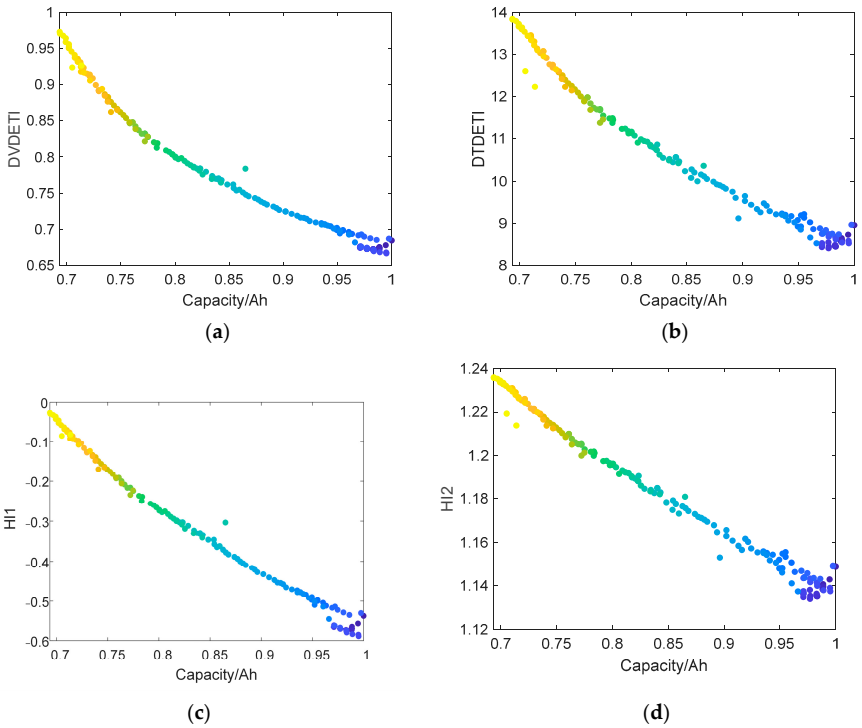

Figure 9. Correlation relationship of the HIs series and capacity for battery #5: (**a**) Scatter plot of raw DVDETI and capacity; (**b**) Scatter plot of DTDETI and capacity; (**c**) Scatter plot of HI1 and capacity; (**d**) Scatter plot of HI2 and capacity.

3.4.2. Quantitative Analysis

For calculating the achievement of the Box-Cox method on the performance of HI1 and HI2, Pearson is used to quantitatively analyze the correlation degree between raw HIs (DVDETI and DTDETI), transformed HIs (HI1 and HI2) and capacity [47]. To research the applicability of HIs, correlation analyses of four batteries are shown in Table 2. As can be seen, the absolute values are close to 1 based on the Pearson method, which means that the HIs are effective, and the time interval chosen in this paper is suitable for different batteries. Compared with DVDETI and DTDETI, HI1 and HI2 have a higher correlation with capacity, which shows that the Box-Cox method is effective in improving the performance of HIs. Therefore, the lithium-ion battery degradation process can be effectively modeled with the transformed HI1 and HI2.

Table 2. Pearson correlation for four batteries.

Battery	HIs			
	HI1	**HI2**	**DVDETI**	**DTDETI**
#5	−0.9945	−0.9934	−0.9777	−0.9838
#6	−0.9874	−0.9766	−0.9694	−0.9679
#7	−0.9928	−0.9803	−0.9849	−0.9789
#18	−0.9867	−0.9762	−0.9790	−0.9707

4. Experimental Results

4.1. Evaluation Indicators

To illustrate the accuracy of the capacity and RUL forecasts in this paper, root mean square error (RMSE) and mean absolute error (MAE) were used as evaluation indicators to make a quantitative assessment for the prediction. The RMSE and MAE are given as

$$RMSE = \sqrt{\frac{\sum_{i=1}^{n}(y_i - \hat{y}_i)^2}{n}} \tag{43}$$

$$MAE = \frac{1}{n}\sum_{i=1}^{n}|y_i - \hat{y}_i| \tag{44}$$

where y_i denotes the true value of HI, and $\hat{y}_i$ is the predicted value of HI.

We also provide the 95% confidence interval (CI) to verify the act of the WOA-MKRVM method. The 95% CI is calculated using

$$95\%CI = \overline{\hat{y}} \pm 1.96 \times cov(\hat{y}) \tag{45}$$

where $\overline{\hat{y}}$ is the mean value of $\hat{y}$, $cov(\hat{y})$ is the covariance of $\hat{y}$.

The absolute error (AE) is an evaluation indicator, which is to evaluate the accuracy of the WOA-MKRVM method for the RUL prediction. The AE can be written as

$$AE = \left|R - \hat{R}\right| \tag{46}$$

where R is the actual life and $\hat{R}$ is the predicted cycle of the lithium-ion battery.

4.2. One-Step Prediction

To explain the performance of the HIs extracted, the one-step prediction on HIs was developed in this paper. One-step prediction means when $k = 1$ in $\hat{Y}_t = \{\hat{H}_{t+k}\}$. The comparison of the before Box-Cox (DVDETI and DTDETI) and after Box-Cox (HI1 and HI2) of battery #5 are presented in Figure 10. The forecast initiate point of battery #5 is cycle 80. The range of DVDETI is greater than 0, and the range of HI1, which after transformation is less than 0. Therefore, the trend of HI1 after normalization is opposite to DVDETI. From Figure 10, it is obvious that the predicted value is close to the truth. In addition, it is obvious that the prediction captures the trend of both the degradation process and regeneration

phenomenon. Moreover, due to the local noise, the prediction results become more accurate when the cycle is close to the start points. HI1 has the best prediction result, which shows that the WOA-MKRVM method is effective. Compared with the before Box-Cox prediction, the results of DVDETI and DTDETI are also relatively accurate, but the accuracy is lower than that of HI1 and HI2, which demonstrates that the Box-Cox method can improve the act of HIs.

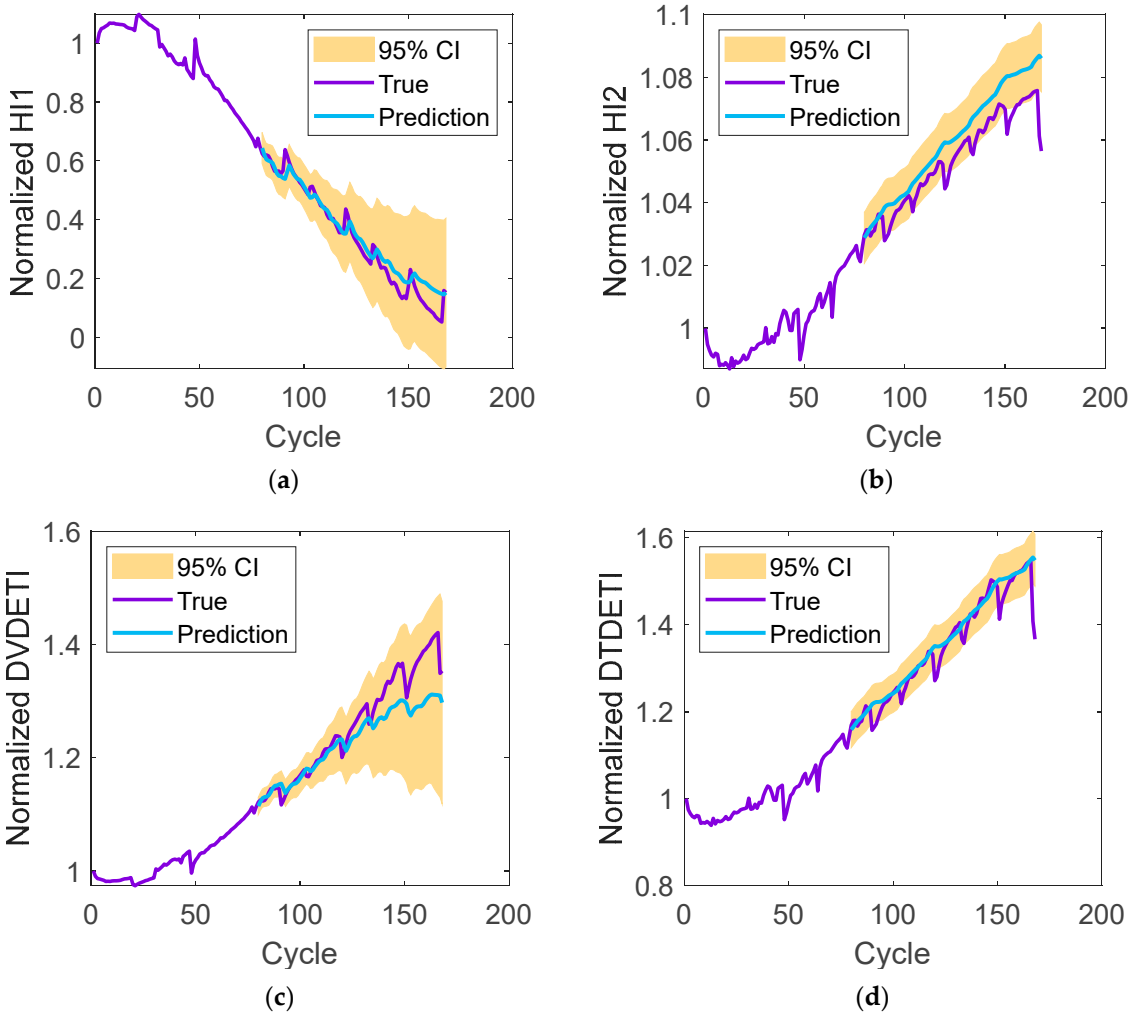

Figure 10. One-step prediction on battery #5: (**a**) HI1; (**b**) HI2; (**c**) DVDETI; (**d**) DTDETI.

The error of the one-step prediction of battery #5 is depicted in Figure 11. It should be pointed out that the error of the result before the transformation is greater than that after the transformation, which shows that the Box-Cox method effectively develops the performance of HIs. The minimal error is the HI2 result for battery #5 and the error of battery #6 is the largest. The reason is that the noise caused by battery #6 has a large fluctuation, and the fluctuation has a large impact on the prediction result. The minimum error of RMSE is the HI2 of battery #18. In addition, the values of MAE are all below 0.05, except DTDETI for battery #6, which indicates that the WOA-MKRVM is more accurate.

Moreover, compared with the prediction result after the box transformation, the result before the box transformation has a larger error which means that Box-Cox is an effective method to improve HI performance.

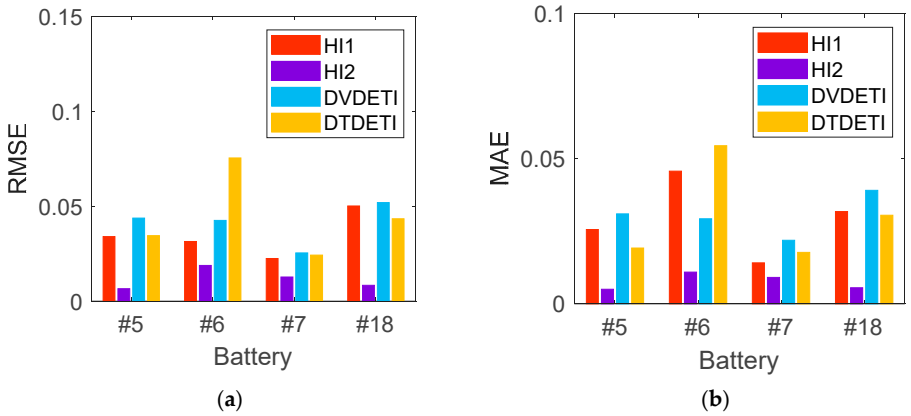

Figure 11. RMSE and MAE of one-step prediction of four batteries: (**a**) RMSE; (**b**) MAE.

4.3. Five-Step Prediction

To explain the robustness of HIs extracted in this paper, the five-step prediction of the HI1, HI2, DVDETI and the DTDETI of four batteries are tested. Also similar to one-step prediction, the five-step prediction means when $k = 5$ in $\hat{Y}_t = \{\hat{H}_{t+k}\}$. The five-step prediction of battery #5 is presented in Figure 12, from which we can conclude that the trend is well predicted, and the predicted result is close to the true value. In addition, the true HIs value is contained in the 95% CI of the predicted result, which shows that WOA-MKRVM has high accuracy. The five-step prediction result of HI2 also follows the same trend as HI1. The true value of the later period is not within the 95% CI of the prediction result. This is because the later period fluctuates greatly, but the model parameters are fixed and insensitive to fluctuations. However, the overall prediction trend is consistent with the true value. Compared with HI1 and HI2, the prediction results of DVDETI and DTDETI clearly deviate from the true value. It can be observed that Box-Cox transformation improves the performance of HIs and enhances prediction accuracy.

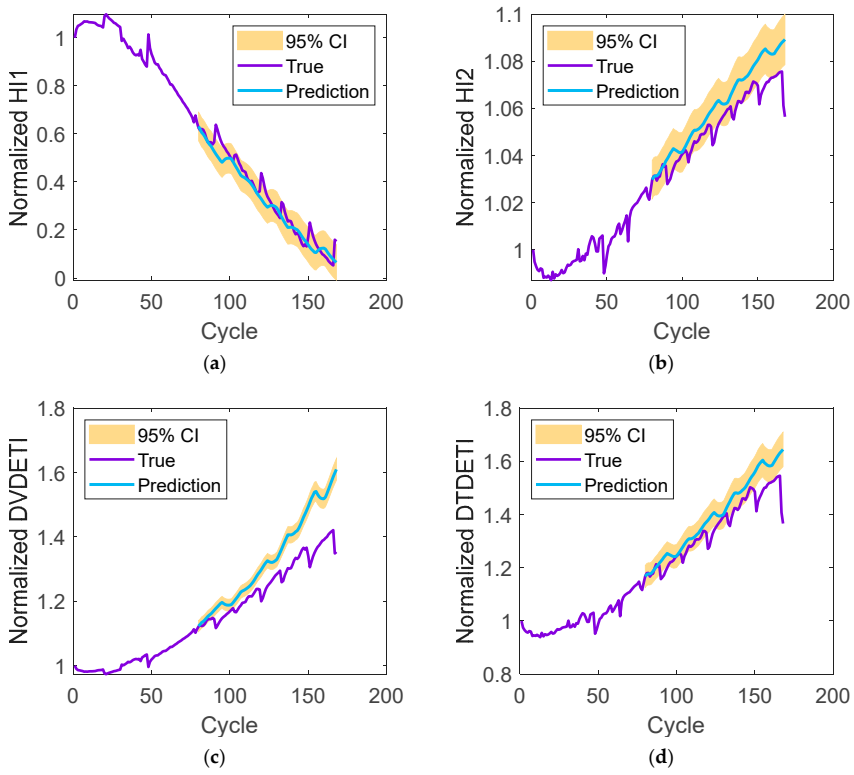

Figure 12. Five-step prediction on battery #5: (**a**) HI1; (**b**) HI2; (**c**) DVDETI; (**d**) DTDETI.

The five-step prediction of RMSE and MAE for four batteries is presented in Figure 13. Figure 13 gives the HI2 prediction of battery #5 and shows minimum RMSE and MAE, while the DVDETI prediction of battery #6 denotes the maximum RMSE and MAE on the four batteries. These results further illustrate that HI1 and HI2 show better prediction performance among the prediction results. Therefore, this comparison further illustrates that the Box-Cox transformation is effective in reinforcing HIs performance and transformed HIs are better for expressing capacity degradation. The largest RMSE and MAE are less than 0.15, and the effectiveness and accuracy of the WOA-MKRVM method for five-step prediction are demonstrated.

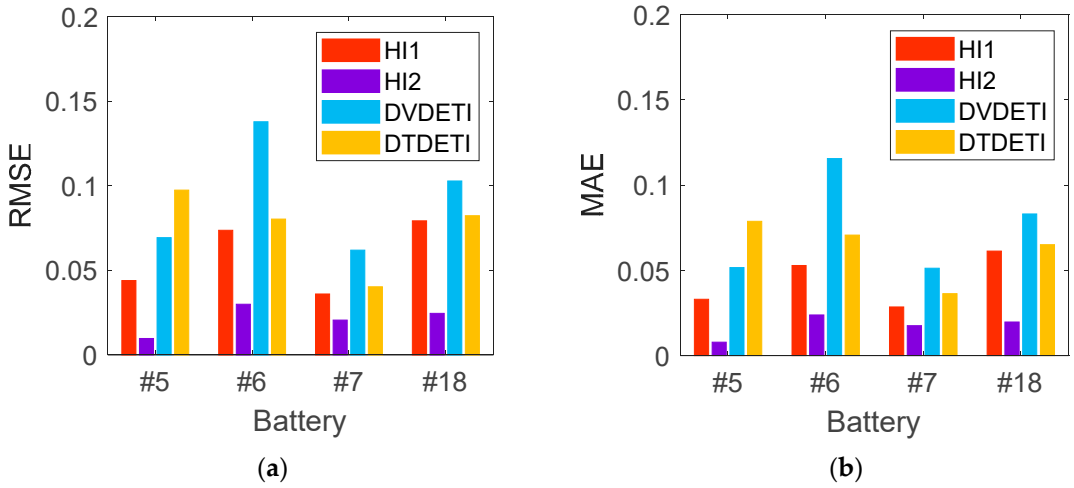

Figure 13. RMSE and MAE of five-step prediction of four batteries: (**a**) RMSE; (**b**) MAE.

4.4. RUL Prediction

4.4.1. RUL Prediction of Different Batteries

To prove the effectiveness of WOA-MKRVM, experiments on three batteries at different starting points were conducted. RUL prediction is an iterative prediction based on one-step prediction. Since battery #7 has not reached the failure threshold of 1.38 Ah, RUL predictions are performed on three batteries #5, #6, and #18. Based on the length of the sample data, the starting points of batteries #5 and #6 are cycles 70, 80, 90, and 100. The starting points of battery #18 are cycles 70, 80, and 90. Moreover, the failure thresholds of the two HIs are calculated according to (40) and (41). The actual thresholds for batteries #5, #6, and #18, which include the capacity and the HIs, are shown in Table 3.

Table 3. Thresholds of capacity and HIs.

Battery	Capacity (Ah)	HI		Actual Cycle Life
		HI1	HI2	
#5	1.38	0.2903	1.0576	128
#6		0.1328	1.2660	112
#18		0.3547	1.0827	100

The RUL prediction results at different cycles for three batteries are presented in Figure 14. For instance, with respect to the RUL prediction result of battery #5 in Figure 14a, it is shown that the prediction can reflect the tendency of the capacity degradation. Due to the fluctuation phenomenon affecting the accuracy of the result, it can also be observed that the prediction result of battery #6 at cycle 80 is better than cycle 70. Another reason is insufficient model training. The earlier starting point has a poor prediction effect, but for the forecast prediction, the later prediction accuracy is more important, and the closer the prediction is to the failure threshold, the more important the result, so that battery health

management can be carried out in advance. The HI2 result of battery #5 is also similar to the HI1.

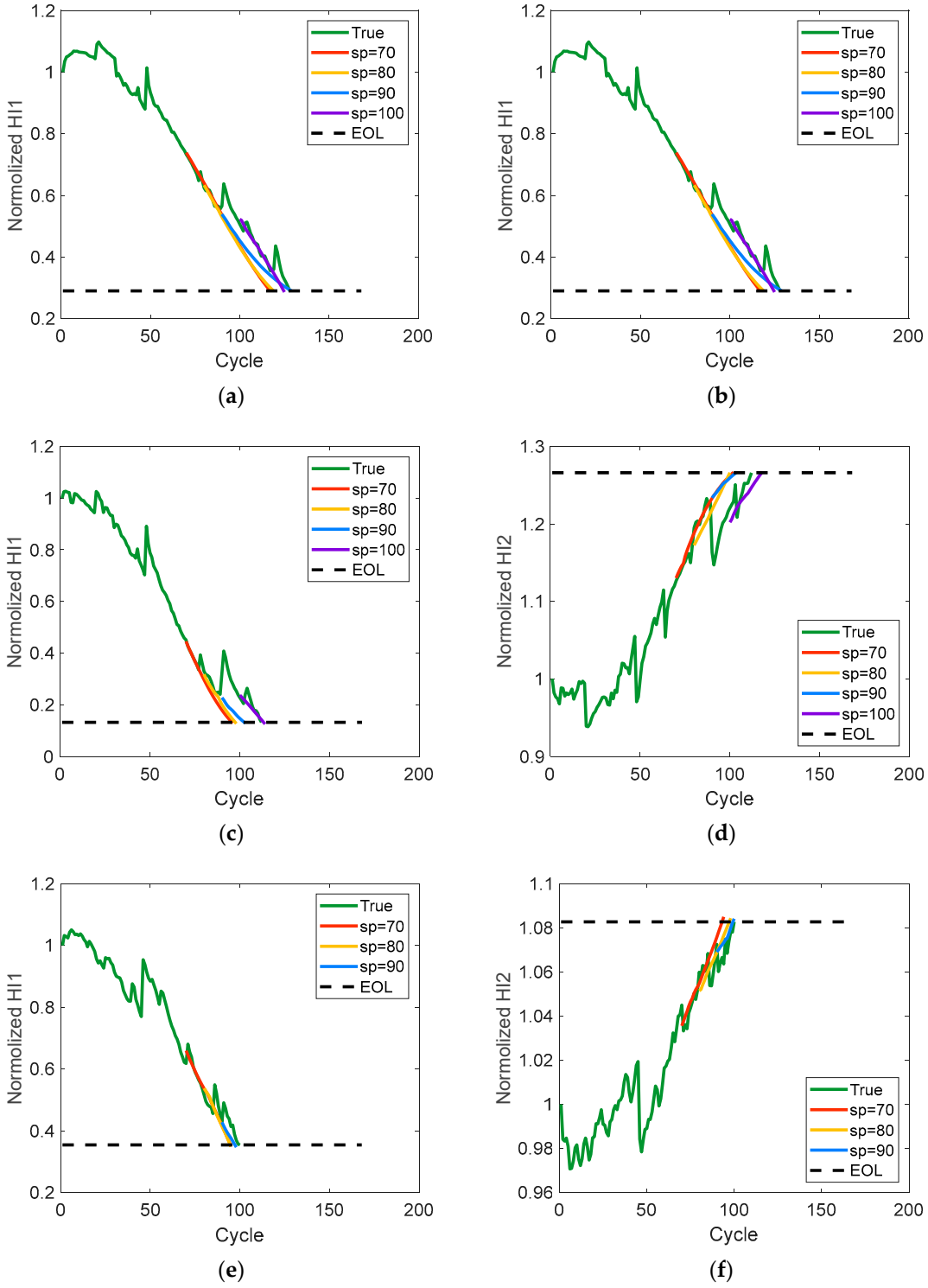

Figure 14. RUL prediction at different starting points on three batteries: (**a**) HI1 of battery #5; (**b**) HI2 of battery #5; (**c**) HI1 of battery #6; (**d**) HI2 of battery #6; (**e**) HI1 of battery #18; (**f**) HI2 of battery #18.

The RUL prediction results based on HI1 and HI2 for batteries #6 and #18 are also similar to battery #5. Compared with battery #18, the performance of battery #6 is not satisfactory. The reason is that large fluctuations in battery #6 in the later period will affect the forecast results. Figure 14e,f is the prediction result of battery #18. It can be observed

that prediction results at different starting points are not much different. This is because the data of battery #18 is less and the starting point is close to the failure threshold. Moreover, it shows that the performance of WOA-MKRVM is relatively powerful and has high accuracy.

Table 4 denotes the HIs RUL prediction error of the three batteries at different starting points. The predicted HI1 values of different starting points for three batteries are between 1 and 15, where the predicted AE value of cycle 70 for battery #6 with the largest prediction error is 15, and the minimum AE of cycle 90 of battery #18 is 1. For the RUL prediction results, it is important that the later cycle prediction accuracy is higher than the previous prediction results. The prediction results of cycles 90 and 100 of the three batteries are ideal. This clearly shows that the real results of the three batteries at different starting points are within the 95% CI of the predicted results, indicating that the WOA-MKRVM has good accuracy. The AE value of HI2 for three batteries is between 1 and 26. The AE value of battery #5 at cycle 70 is the largest. This is because the model parameters relative to battery # 5 is not suitable, the error is larger than other batteries, but the error is reduced after cycle 90, and the prediction result is still satisfactory.

Table 4. RUL estimation of three batteries.

Battery	Start Points	HI	Actual RUL	Predicted RUL	95% CI	AE
#5	70	HI1	58	48	[39,64]	10
		HI2		32	[26,39]	26
	80	HI1	48	40	[31,58]	8
		HI2		27	[21,34]	21
	90	HI1	38	40	[27,72]	2
		HI2		42	[17,52]	4
	100	HI1	28	26	[20,32]	2
		HI2		22	[14,30]	6
#6	70	HI1	42	27	[18,-]	15
		HI2		33	[17,-]	9
	80	HI1	32	19	[11,34]	13
		HI2		21	[12,31]	11
	90	HI1	22	14	[4,32]	8
		HI2		15	[1,23]	7
	100	HI1	12	15	[6,24]	3
		HI2		19	[4,34]	7
#18	70	HI1	30	26	[17,35]	4
		HI2		25	[13,34]	5
	80	HI1	20	16	[9,23]	4
		HI2		19	[8,29]	1
	90	HI1	10	9	[1,15]	1
		HI2		11	[1,22]	1

Compared with HI1, the HI2 prediction results are better for six groups and only have decreased performance for the other four cases, and one group of results is equal to the predicted results. The error value of RUL obtained with HI1 and HI2 may result from local regeneration and various fluctuations, but the prediction results are very satisfactory. In conclusion, the proposed HIs in this paper are effective for lithium-ion battery RUL prediction.

4.4.2. Comparisons with Related Studies

To verify the accuracy of WOA-MKRVM, it is necessary to present a comparison of the RUL prediction results of WOA-MKRVM and methods in other studies. This paper selects literature with the same prediction starting point for comparison. To avoid the duplicate description of results, Table 5 contains a comparison of the RUL results of different methods. Compared with one study [16], the capability of WOA-MKRVM in this paper is more stable. The result of cycle 80 in [16] is the smallest and the result of battery #18 is better than

the HI2 prediction in this paper. However, the performances of WOA-MKRVM in other cases are more satisfactory. Compared with [17], it can be seen that the HI1 prediction in this paper is only worse in the result of battery #6 at cycle 100. Moreover, it is obvious that superior performance is achieved by WOA-MKRVM in other terms, and the same patterns are also found in HI2 prediction. However, compared with the WOA-MKRVM, the predictions of the other cycles in [47] are not accurate. Accordingly, the effectiveness and accuracy of WOA-MKRVM on lithium-ion battery RUL predictions is verified.

Table 5. RUL prediction comparisons with related studies.

Start Points	Battery								
	#5			#6			#18		
	[16]	[17]	[48]	[16]	[17]	[48]	[16]	[17]	[48]
70	19	18	N/A	18	23	N/A	5	7	N/A
80	2	14	12	2	16	10	1	5	1
90	15	13	N/A	16	14	N/A	4	4	N/A
100	12	10	8	3	1	3	N/A	N/A	N/A

5. Conclusions

Knowing the RUL in advance is vital for the stable performance of the lithium-ion-battery-powered system. This paper proposes raw HIs (DVDETI and DTDETI) to demonstrate the degradation state of lithium-ion batteries, and uses Box-Cox transformed HIs (HI1 and HI2) to improve the linear relationship between capacity and raw HIs. The WOA-MKRVM model is applied for predicting capacity degradation and RUL. The probability results based on battery data show that the after-Box-Cox-transformed HI1 and HI2 are effective and accurate. It is remarkable that the limitation of HIs in this paper is that it only examines the partial discharging process information changes at specific time periods, which include voltage and temperature, and the factors of the charging process are also worth considering. In our future work, robust and effective HIs suitable for different operations should be studied, which can be generally applied for online RUL prediction. Moreover, combining the data-driven method with other methods (e.g., particle filter) can be considered for developing the accuracy and generalization of the prognostic for lithium-ion batteries. The prediction of the two HIs provide guidance for the safe management of lithium-ion batteries, and this method is also transferable and can be migrated to use with other available HIs.

Author Contributions: Conceptualization, Y.Y. and J.W. (Jie Wen); methodology, Y.Y. and J.W (Jie Wen).; software, Y.Y.; validation, Y.Y. and J.W. (Jie Wen); formal analysis, Y.Y.; investigation, Y.Y. and J.W. (Jie Wen); writing—original draft preparation, Y.Y.; writing—review and editing, J.W. (Jie Wen); visualization, Y.Y., J.L. and J.W (Jiang Wang); supervision, J.W. (Jie Wen), J.L. and Y.T.; project administration, J.W. (Jie Wen) and Y.S.; funding acquisition, J.W. (Jie Wen). All authors have read and agreed to the published version of the manuscript.

Funding: This work was funded by the National Natural Science Foundation of China, grant number 72071183, and Shanxi Scholarship Council of China, grant number 2020-114.

Institutional Review Board Statement: Not applicable.

Informed Consent Statement: Not applicable.

Data Availability Statement: No new data were created or analyzed in this study. Data sharing is not applicable to this article.

Acknowledgments: The authors would like to thank the NASA Ames Center of Excellence Diagnostic Center for providing the experimental data.

Conflicts of Interest: The authors declare no conflict of interest.

References

1. Lipu, M.S.H.; Hannan, M.A.; Hussain, A.; Hoque, M.M.; Ker, P.J.; Saad, M.H.M.; Ayob, A. A Method for Battery Health Estimation Based on Charging Time Segment. *J. Clean. Prod.* **2018**, *205*, 115–133. [CrossRef]
2. Li, Y.; Liu, K.; Foley, A.M.; Zülke, A.; Berecibar, M.; Nanini-Maury, E.; Van Mierlo, J.; Hoster, H.E. Data-driven health estimation and lifetime prediction of lithium-ion batteries: A review. *Renew. Sustain. Energy Rev.* **2019**, *113*, 109254. [CrossRef]
3. Meng, H.; Li, Y.-F. A review on prognostics and health management (PHM) methods of lithium-ion batteries. *Renew. Sustain. Energy Rev.* **2019**, *116*, 109405. [CrossRef]
4. Guha, A.; Patra, A. Online Estimation of the Electrochemical Impedance Spectrum and Remaining Useful Life of Lithium-Ion Batteries. *IEEE Trans. Instrum. Meas.* **2018**, *67*, 1836–1849. [CrossRef]
5. Peng, J.; Zhou, Z.B.; Wang, J.Q.; Wu, D.; Guo, Y.M. Residual Remaining Useful Life Prediction Method for Lithium-Ion Batteries in Satellite with Incomplete Healthy Historical Data. *IEEE Access* **2019**, *7*, 127788–127799. [CrossRef]
6. Song, Y.C.; Liu, D.T.; Yang, C.; Peng, Y. Data-driven hybrid remaining useful life estimation approach for spacecraft lithium-ion battery. *Microelectron. Reliab.* **2017**, *75*, 142–153. [CrossRef]
7. Li, X.Y.; Shu, X.; Shen, J.W.; Xiao, R.X.; Yan, W.S.; Chen, Z. An On-Board Remaining Useful Life Estimation Algorithm for Lithium-Ion Batteries of Electric Vehicles. *Energies* **2017**, *10*, 691. [CrossRef]
8. Prada, E.; Di Domenico, D.; Creff, Y.; Bernard, J.; Sauvant-Moynot, V.; Huet, F. Simplified Electrochemical and Thermal Model of LiFePO4-Graphite Li-Ion Batteries for Fast Charge Applications. *J. Electrochem. Soc.* **2012**, *159*, A1508–A1519. [CrossRef]
9. Thomas, E.V.; Bloom, I.; Christophersen, J.P.; Battaglia, V.S. Rate-based degradation modeling of lithium-ion cells. *J. Power Sources* **2012**, *206*, 378–382. [CrossRef]
10. Li, W.H.; Fan, Y.; Ringbeck, F.; Jost, D.; Han, X.B.; Ouyang, M.G.; Sauer, D.U. Electrochemical model-based state estimation for lithium-ion batteries with adaptive unscented Kalman filter. *J. Power Sources* **2020**, *476*, 13. [CrossRef]
11. Li, Y.; Wei, Z.; Xiong, B.; Vilathgamuwa, D.M. Adaptive Ensemble-Based Electrochemical—Thermal Degradation State Estimation of Lithium-Ion Batteries. *IEEE Trans. Ind. Electron.* **2022**, *69*, 6984–6996. [CrossRef]
12. Chen, L.; Zhang, Y.; Zheng, Y.; Li, X.; Zheng, X. Remaining useful life prediction of lithium-ion battery with optimal input sequence selection and error compensation. *Neurocomputing* **2020**, *414*, 245–254. [CrossRef]
13. Ren, L.; Zhao, L.; Hong, S.; Zhao, S.Q.; Wang, H.; Zhang, L. Remaining Useful Life Prediction for Lithium-Ion Battery: A Deep Learning Approach. *IEEE Access* **2018**, *6*, 50587–50598. [CrossRef]
14. Zhang, Y.Z.; Xiong, R.; He, H.W.; Pecht, M.G. Long Short-Term Memory Recurrent Neural Network for Remaining Useful Life Prediction of Lithium-Ion Batteries. *IEEE Trans. Veh. Technol.* **2018**, *67*, 5695–5705. [CrossRef]
15. Yu, W.N.; Kim, I.Y.; Mechefske, C. Remaining useful life estimation using a bidirectional recurrent neural network based autoencoder scheme. *Mech. Syst. Signal Process.* **2019**, *129*, 764–780. [CrossRef]
16. Zhang, W.; Li, X.; Li, X. Deep learning-based prognostic approach for lithium-ion batteries with adaptive time-series prediction and on-line validation. *Measurement* **2020**, *164*, 108052. [CrossRef]
17. Yu, J. State of health prediction of lithium-ion batteries: Multiscale logic regression and Gaussian process regression ensemble. *Reliab. Eng. Syst. Saf.* **2018**, *174*, 82–95. [CrossRef]
18. Jia, J.; Liang, J.; Shi, Y.; Wen, J.; Pang, X.; Zeng, J. SOH and RUL Prediction of Lithium-Ion Batteries Based on Gaussian Process Regression with Indirect Health Indicators. *Energies* **2020**, *13*, 375. [CrossRef]
19. Li, H.; Pan, D.; Chen, C.L.P. Intelligent Prognostics for Battery Health Monitoring Using the Mean Entropy and Relevance Vector Machine. *IEEE Transactions on Syst. Man Cybern. Syst.* **2014**, *44*, 851–862. [CrossRef]
20. Sun, Y.; Hao, X.; Pecht, M.; Zhou, Y. Remaining useful life prediction for lithium-ion batteries based on an integrated health indicator. *Microelectron. Reliab.* **2018**, *88–90*, 1189–1194. [CrossRef]
21. Zhao, Q.; Qin, X.; Zhao, H.; Feng, W. A novel prediction method based on the support vector regression for the remaining useful life of lithium-ion batteries. *Microelectron. Reliab.* **2018**, *85*, 99–108. [CrossRef]
22. Widodo, A.; Shim, M.-C.; Caesarendra, W.; Yang, B.-S. Intelligent prognostics for battery health monitoring based on sample entropy. *Expert Syst. Appl.* **2011**, *38*, 11763–11769. [CrossRef]
23. Zhang, C.; He, Y.; Yuan, L.; Xiang, S. Capacity Prognostics of Lithium-Ion Batteries using EMD Denoising and Multiple Kernel RVM. *IEEE Access* **2017**, *5*, 12061–12070. [CrossRef]
24. Zheng, X.J.; Fang, H.J. An integrated unscented kalman filter and relevance vector regression approach for lithium-ion battery remaining useful life and short-term capacity prediction. *Reliab. Eng. Syst. Saf.* **2015**, *144*, 74–82. [CrossRef]
25. Li, Z.X.; Goebel, K.; Wu, D.Z. Degradation Modeling and Remaining Useful Life Prediction of Aircraft Engines Using Ensemble Learning. *J. Eng. Gas Turbines Power-Trans. Asme* **2019**, *141*, 041008. [CrossRef]
26. Liu, D.; Zhou, J.; Liao, H.; Peng, Y.; Peng, X. A Health Indicator Extraction and Optimization Framework for Lithium-Ion Battery Degradation Modeling and Prognostics. *IEEE Trans. Syst. Man Cybern.-Syst.* **2015**, *45*, 915–928. [CrossRef]
27. Ma, S.; Jiang, M.; Tao, P.; Song, C.; Wu, J.; Wang, J.; Deng, T.; Shang, W. Temperature effect and thermal impact in lithium-ion batteries: A review. *Prog. Nat. Sci. Mater. Int.* **2018**, *28*, 653–666. [CrossRef]
28. Ruiz, V.; Kriston, A.; Adanouj, I.; Destro, M.; Fontana, D.; Pfrang, A. Degradation Studies on Lithium Iron Phosphate—Graphite Cells. The Effect of Dissimilar Charging—Discharging Temperatures. *Electrochim. Acta* **2017**, *240*, 495–505. [CrossRef]
29. Lu, Z.; Yu, X.L.; Wei, L.C.; Cao, F.; Zhang, L.Y.; Meng, X.Z.; Jin, L.W. A comprehensive experimental study on temperature-dependent performance of lithium-ion battery. *Appl. Therm. Eng.* **2019**, *158*, 113800. [CrossRef]

30. Tang, X.; Wang, Y.; Zou, C.; Yao, K.; Xia, Y.; Gao, F. A novel framework for Lithium-ion battery modeling considering uncertainties of temperature and aging. *Energy Convers. Manag.* **2019**, *180*, 162–170. [CrossRef]
31. Kong, J.-Z.; Yang, F.; Zhang, X.; Pan, E.; Peng, Z.; Wang, D. Voltage-temperature health feature extraction to improve prognostics and health management of lithium-ion batteries. *Energy* **2021**, *223*, 120114. [CrossRef]
32. Sakia, R. The Box-Cox Transformation Technique: A Review. *Statistician* **1992**, *41*, 169–178. [CrossRef]
33. Zhang, Y.; Xiong, R.; He, H.; Pecht, M.G. Lithium-Ion Battery Remaining Useful Life Prediction With Box-Cox Transformation and Monte Carlo Simulation. *IEEE Trans. Ind. Electron.* **2019**, *66*, 1585–1597. [CrossRef]
34. Tipping, M. Sparse Bayesian Learning and the Relevance Vector Machine. *J. Mach. Learn. Res.* **2001**, *1*, 211–244. [CrossRef]
35. Blekas, K.; Likas, A. Sparse regression mixture modeling with the multi-kernel relevance vector machine. *Knowl. Inf. Syst.* **2013**, *39*, 241–264. [CrossRef]
36. Wang, H.; Xu, D.; Martinez, A. Parameter selection method for support vector machine based on adaptive fusion of multiple kernel functions and its application in fault diagnosis. *Neural Comput. Appl.* **2020**, *32*, 183–193. [CrossRef]
37. Cheng, K.; Lu, Z.; Wei, Y.; Shi, Y.; Zhou, Y. Mixed kernel function support vector regression for global sensitivity analysis. *Mech. Syst. Signal Process.* **2017**, *96*, 201–214. [CrossRef]
38. Li, X.; Wang, Z.; Yan, J. Prognostic health condition for lithium battery using the partial incremental capacity and Gaussian process regression. *J. Power Sources* **2019**, *421*, 56–67. [CrossRef]
39. Liu, Y.F.; Zhao, G.Q.; Peng, X.Y. Deep Learning Prognostics for Lithium-Ion Battery Based on Ensembled Long Short-Term Memory Networks. *IEEE Access* **2019**, *7*, 155130–155142. [CrossRef]
40. Sun, Y.; Yang, T.; Liu, Z. A whale optimization algorithm based on quadratic interpolation for high-dimensional global optimization problems. *Appl. Soft Comput.* **2019**, *85*, 105744. [CrossRef]
41. Mehne, H.H.; Mirjalili, S. A parallel numerical method for solving optimal control problems based on whale optimization algorithm. *Knowl.-Based Syst.* **2018**, *151*, 114–123. [CrossRef]
42. Mirjalili, S.; Lewis, A. The Whale Optimization Algorithm. *Adv. Eng. Softw.* **2016**, *95*, 51–67. [CrossRef]
43. Saha, B.G.K. Battery Data Set: NASA Ames Prognostics Data Repository. Available online: https://ti.arc.nasa.gov/tech/dash/groups/pcoe/prognostic-data-repository/ (accessed on 18 February 2020).
44. Xiong, R.; Pan, Y.; Shen, W.; Li, H.; Sun, F. Lithium-ion battery aging mechanisms and diagnosis method for automotive applications: Recent advances and perspectives. *Renew. Sustain. Energy Rev.* **2020**, *131*, 110048. [CrossRef]
45. Barré, A.; Suard, F.; Gérard, M.; Montaru, M.; Riu, D. Statistical analysis for understanding and predicting battery degradations in real-life electric vehicle use. *J. Power Sources* **2014**, *245*, 846–856. [CrossRef]
46. Cardoso, G.; Brouhard, T.; DeForest, N.; Wang, D.; Heleno, M.; Kotzur, L. Battery aging in multi-energy microgrid design using mixed integer linear programming. *Appl. Energy* **2018**, *231*, 1059–1069. [CrossRef]
47. Nahler, G. Pearson correlation coefficient. In *Dictionary of Pharmaceutical Medicine*; Nahler, G., Ed.; Springer: Vienna, Austria, 2009; p. 132.
48. Zhang, L.; Mu, Z.; Sun, C. Remaining Useful Life Prediction for Lithium-Ion Batteries Based on Exponential Model and Particle Filter. *IEEE Access* **2018**, *6*, 17729–17740. [CrossRef]